Confocal fluorescence imaging of photosensitised DNA denaturation in cell nuclei

Tytus Bernas [1,2] , Elikplimi K. Asem [3], J. Paul Robinson [3], Peter R.Cook [4], Jurek W.Dobrucki [1]

[1] Laboratory of Confocal Microscopy and Image Analysis, Department of Biophysics, Faculty of Biotechnology, Jagiellonian University, Gronostajowa 7, 30-387 Krakow, Poland

[2] University of Silesia, Department of Plant Anatomy and Cytology, Faculty of Biology and Protection of Environment, Jagiellonska 28, Katowice, Poland

[3] Purdue University, Department of Basic Medical Sciences, 625 Harrison St. West Lafayette, IN, 47907, USA

[4] Oxford University, Sir William Dunn School of Pathology, South Parks Road, Oxford OX1 3RE, UK

Correspondence:
Jurek W.Dobrucki

Laboratory of Confocal Microscopy and Image Analysis, Department of Biophysics, Faculty of Biotechnology, Jagiellonian University, Gronostajowa 7, 30-387 Krakow, Poland; dobrucki@mol.uj.edu.pl
Tel. +48 12 / 664 6382
Fax. +48 12 / 664 6902

Abstract

The double stranded helical structure of DNA is maintained in part by hydrogen bonds between strands and stacking interactions between adjacent purine and pyrimidine bases in one strand. The transition (denaturation) from double stranded (ds) to single-stranded (ss) can be induced in isolated DNA or fixed cells by exposure to elevated temperatures, alkali or acids, aprotic or nonpolar solvents or some drugs. We report here that DNA denaturation can occur *in situ*, in cell nuclei, as a result of interaction between light and an intercalated dye, acridine orange or ethidium bromide. This DNA photodenaturation was probed using metachromatic properties of acridine orange and imaged by fluorescence confocal microscopy. Furthermore, an empirical kinetic model was developed to separate changes of acridine orange luminescence intensities caused by photobleaching from those, which were a result of DNA denaturation. We investigated the influence of oxygen on these phenomena and propose mechanism by which photodenaturation may occur.

Keywords

DNA denaturation, confocal microscopy, acridine orange, photobleaching

Introduction

Denaturation of nucleic acids

The double stranded helical structure of DNA is maintained in part by hydrogen bonds between strands and stacking interactions between adjacent purine and pyrimidine bases in one strand (1, 2). It is thought that DNA double helix constantly 'breaks' as the two strands separate. Moreover, DNA in the nuclei of living cells becomes single-stranded (ss) during replication, transcription and repair. Disruption of the native structure may also result from modifications of the bases or sugar backbone induced by chemicals or light. In living cells such changes are reversed by specialised enzymatic systems responsible for preventing loss of genetic information (3). Denaturation can be induced in isolated DNA or in fixed cells by exposure to elevated temperatures (4), alkali or acids (5, 6), aprotic or nonpolar solvents (7, 8) or some drugs (9). Denaturation forms part of some labelling protocols, including FISH (7) and immunostaining of incorporated BrdU (10).

We report here that the DNA double helix can be split into separate strands as a result of interaction between light and an intercalated dye. This observation may be relevant to understanding mechanisms of DNA damage inflicted by visible light. This phenomenon may also be exploited to denature DNA locally in selected regions of nuclei in living cells to study the repair and remodelling of DNA.

Detection of in situ denaturation of DNA

Single and double stranded nucleic acids in cells can be detected with acridine orange (AO). The dye binds to DNA of G_0/G_1 cells in a stoichiometric manner (9). Binding is not affected by the degree of chromatin condensation or base composition (with the exception for A/T stretches) (9). AO exhibits two types of binding - intercalation of monomers to ds nucleic acids, and dye-base stacking

with ss nucleic acids (Fig. 1). Intercalation results in green fluorescence (excitation max. 502 nm, emission max. 522 nm), whereas dye stacks emit red luminescence (excitation max. 457 nm, emission max. 638 nm) (9, 11). Thus, the degree of denaturation can be followed by measuring intensities of luminescence in these two spectral regions (4, 6, 12, 13). However, accurate measurements of the ratio between these two emissions require that light-induced degradation of AO (photobleaching) is prevented, or at least accounted for.

In this report we describe detection of the denaturation of DNA induced by the illumination of bound AO. Denaturation is detected by confocal fluorescence microscopy and we constructed an empirical kinetic model explaining the observations.

Materials and Methods

Reagents. Acridine orange (AO) and Hoechst 33342 were obtained from Molecular Probes (Eugene, OR, USA), ribonuclease A (RNase) and ethidium bromide (EB) from Sigma-Aldrich, formaldehyde (16% EM Grade) from Electron Microscopy Sciences (Ft Washington, PA, USA). Stocks of AO and EB were made in PBS and kept at 4^{o}C; stocks of RNase were kept frozen. Compressed argon (BOC Gazy, Poland) was 99.998% pure; the gas was delivered to an imaged sample through copper and steel tubes.

Cell cultures MSU 1.1 human fibroblasts (14) were cultured on 20 mm diameter, 0.17 mm thick coverslips (Menzel, Braunschweig, Germany) placed in tissue culture Petri dishes (TPP, Switzerland). DMEM (Sigma) supplemented with 10% foetal bovine serum (Gibco) and antibiotics was used. Confluent monolayers (two days after seeding) were used in all experiments. Cell density was approximately 1100 cells/mm^{2}. The cells were counted manually on coverslips under a 60x objective (field 173.25 um x 173.25 μm) in wide-field DIC mode. The reported density is an average of 25 fields distributed between 5 coverslips.

Fixation and fluorescent labelling. Coverslips with live cells were washed 3x with PBS (with Mg^{+2} and Ca^{+2}), and fixed with formaldehyde (1% in PBS at 20˚ for 1 h). Coverslips with fixed cell cultures were mounted in a round steel holder using silicone grease. The preparations were incubated in RNase (0.5 mg/ml in PBS) for 4 h at room temperature and washed 3x with PBS. The holder was fitted in a microscope stage microincubator (Life Sci. Res., Cambridge, UK). Nuclei of MSU 1.1 cells were stained by 45 min incubation with a solution of AO (10 μg/ml) in PBS. The AO concentration was chosen to provide conditions for formation of AO aggregates on single-stranded DNA and differential staining of single-stranded and double-stranded DNA. The titration and careful study of AO interaction with DNA was published by Darzynkiewicz and Kapuscinski (4, 9). Following

incubation with AO, the dye solution was removed and the preparation was incubated in fresh PBS for 30 min prior to imaging.

Confocal microscopy. Experiments were carried out using a BioRad MRC1024 confocal system (BioRad, Hemel Hempstead, UK) equipped with a Nikon Diaphot 300 microscope (Nikon, Amsterdam), 60x PlanApo oil immersion objective lens (NA 1.4), 100 mW air-cooled argon ion VIS laser (ILT, Salt Lake City, UT, USA) and a 250 mW water-cooled argon ion UV laser (Coherent Inc. Santa Clara, CA, USA). AO, EB, and Hoechst were excited with 457, 514 and 351 nm laser lines, respectively. A 510 long pass primary dichroic mirror (VHS filter block) was used for excitation of EB and AO; whereas 380-450 band pass/500 long pass primary multichroic (UHBS) was used to excite Hoechst. Fluorescence of AO monomers (490 - 550 nm) and luminescence of AO aggregates (640 – 700 nm) was detected using a 522/30 band pass and 640 long pass filter, respectively.

Time series of fluorescent confocal images of equatorial sections through nuclei (thickness approx. 1.1 μm, positioned 2.0 - 2.5 μm above the coverslip) were collected using alternately a small-intensity probing beam and a large-intensity bleaching beam. No measurable bleaching occurred when labels were excited using the probing beam alone. The confocal pinholes were adjusted using a calibration curve generated with aqueous solution of fluorescein as the standard, so that the optical section thickness was the same in the green and the red luminescence detection bands. The sizes of the pinholes were 2.0 mm (2.4 Airy units) and 1.9 mm (1.8 Airy units) in the green and the red bands, respectively. The total incident power was measured at 457 nm and 514 nm lines of the VIS (air-cooled) Ar ion laser using a power meter (LaserCheck, Coherent Inc.) positioned at the exit pupil of the objective. The power (adjusted using neutral density filters of 1, 10, 30 or 100% transmission) was: 0.03 mW for the 457 nm (AO) probing beam, 0.3-3 mW for the 457 nm (AO) bleaching beam, 3 mW for 514 nm (EB) bleaching beam. The intensity of the 351 nm bleaching beam (Hoechst) was 10 mW. The light flux, expressed as an average for one image

(scan), was 0.11 W/cm^2 (the AO probing beam) and 1.11 - 11.1 W/cm^2 (the AO bleaching beam). Maximum instantaneous energy flux at the central area (Airy disc) of the diffraction limited PSF (effective NA=1.23) at the focal plane was 13.4 W/cm^2 (AO probing beam) and 134 – 1336 W/cm^2 (AO bleaching beam). The maximum flux was 4.9 times lower at the horizontal borders of the optical section, as calculated using PSF modelled with Xcosm (IBC, Washington University, St. Louis, USA). Images (512 x 512 pixels; 256 grey levels) were collected (either with the probing or the bleaching beam) using LaserSharp 3.2 software (Bio-Rad). One image was a sum of 20 consecutive scans (3.5s each). Size of a pixel was 0.338 μm (zoom 1.0) unless otherwise stated. The average pixel dwell time was 13 μs. Fluorescence was detected using photomultipliers in photon-counting mode. The maximum number of photons detected in a scan did not exceed 13, which was well below detector saturation. During image registration the sample was in equilibrium with atmospheric air or argon, as indicated. Experiments were performed 3 – 6 times in each set of conditions and 45 – 90 nuclei were analysed.

Removal of oxygen. To remove oxygen from samples the microincubator was closed with a glass cover and pure argon was bubbled through the PBS covering the cells for 30 min prior to, and during image collection. Control experiments with an oxygen-sensitive luminescent probe – $Ru(phen)_3^{2+}$ (6, 15) – confirmed that oxygen had been removed.

Denaturation of DNA with formamide. Cells were stained with AO as described before. Subsequently, staining solution was withdrawn and replaced with formamide for 30 min. Next, formamide was removed, cells rinsed three times with PBS, and incubated in PBS supplemented with 10 μg/ml acridine orange for 60 min. In control experiments formamide was replaced with PBS.

Photodenaturation with EB and Hoechst. Cells were cultured and fixed as described before and incubated with EB (5 μg/ml in PBS) or Hoechst 33342 (5

μg/ml in PBS) for 30 min. To check if EB fluorescence would interfere with measurements of AO luminescence, the EB stained cells were imaged using the standard AO instrument settings (probing beam). No signal was detected in the range of 490 - 550 nm (green AO fluorescence), whereas signal intensity in the range of 640 – 700 nm was not higher than 5% of red luminescence usually detected in AO-stained cells. No Hoechst fluorescence was detectable using these instrument settings. Subsequently, cells were illuminated using 514 nm (average flux 15.6 W/cm^2, average dose 3.6 kJ/cm^2) or 351 nm (flux 34.7 W/cm^2, dose 4.4 kJ/cm^2) light as a bleaching beam for EB or Hoechst, respectively. Following bleaching, the cells were rinsed three times with PBS and incubated in PBS supplemented with 10 μg/ml AO. Green and red emissions of AO were imaged to detect DNA denaturation (6). Samples incubated without EB and Hoechst served as controls.

Analysing kinetics of luminescence intensity change. Time series of 2D image stacks (registered using the probing beam) were converted to sets of 8-bit uncompressed tiff files (one set per a detection channel), transformed back to the form of stack with Matlab 5.2 and pre-processed using a median filter (square mask 3x3). Only pixels with an initial brightness of $\geq$6 on the grey scale were analysed. The grey scale was subdivided into 25 consecutive intervals (i.e., from 6-15, 16-25, etc.) using binary masks. The masks were constructed from first images (i.e. registered before bleaching) in the respective sets for the calculation of photobleaching of the two AO forms. The masks based on images of monomeric AO fluorescence were used to quantitate the increase of aggregate AO luminescence resulting from photodenaturation. Average intensities of pixels comprising each brightness class were calculated for each of the images in the stack, before background (the mean intensity of signal in an area without cells) was subtracted. These corrected values were plotted against the total dose (J/cm^2) of the incident light and the number of scans (see Results, loss of green and red luminescence of AO). Additional correction for photobleaching was applied in the case of photodenaturation analysis (see Results, red AO

luminescencein initially green areas) before constructing plots, as described further in this section.

Calculation of photobleaching rates and apparent reaction orders. The method used was adopted from (16) and described in detail in (17). Briefly, bi-exponential functions, described by the following general equation:

$$I(w) = Ae^{-Bw} + Ce^{-Dw} \qquad \text{eq. 1}$$

where: I – fluorescence intensity; w – total incident excitation light dose; A,B,C,D - phenomenological coefficients

were fitted to kinetic curves of AO monomer bleaching. Alternatively, linear functions:

$$I(w) = Aw + B \qquad \text{eq. 2}$$

where: I , w, A, B as before

were fitted to kinetic curves of AO aggregate bleaching. Subsequently the initial absolute rates of photobleaching (R_a - loss of fluorescence measured in arbitrary units divided by light dose) were calculated using the first derivatives (taken at 0) of the fitted functions (eq. 1 and 2):

$$R_a = \left.\frac{dI}{dw}\right|_{w=0} \qquad \text{eq. 3}$$

where: I , w, as before

Hence, the apparent order of photobleaching reaction (α) was calculated from the slope of the plot of logarithm of absolute photobleaching rate against excitation light flux:

$$\ln(R_a J) = \alpha \ln(J) + \ln(b) \qquad \text{eq 4}$$

where: b – constant, J – excitation light flux

Calculation of photodenaturation rates and apparent reaction orders Pixel intensities in the time series of AO aggregate luminescence images were corrected for photobleaching on pixel-by-pixel basis using the following formula:

$$I^{c}_{n} = I_{n} + R_{a}(I_{0})w \qquad \text{eq. } 5$$

where: I_n and I^c_n – raw and corrected pixel intensity in n-th image, $R_a(I_0)$ – absolute photobleaching rate for initial pixel intensity (I_0), w – total incident light dose.

These corrected values were plotted against the total dose (J/cm^2) of the incident light and the number of scans, as previously. Linear functions (see eq. 2) were fitted to these fragments of the kinetic curves where an increase of intensity was detectable (i.e. from the third image on). Absolute rates of intensity increase (photodenaturation rates) were calculated using eq 3.

Results

Detection of DNA denaturation by AO

AO binds to nucleic acids by intercalation and base stacking (9, 4). The predominant mode of binding is dependent on the concentration of AO (or more precisely, the dye:nucleic acid ratio). At a concentration of 5-10 µg/ml, AO binds differentially to single-stranded (ss) and double-stranded (ds) nucleic acids (9, 11) (Fig. 1). In the former case it tends to aggregate (stack) and emit red luminescence, whereas in the latter it intercalates and fluoresces green. It is, thus, reasonable to expect that denaturation of dsDNA will decrease intercalative binding of monomeric AO and increase binding of the stacked, aggregated AO. When fixed MSU human fibroblasts were stained with AO and exposed to formamide, red luminescence increased, while green fluorescence decreased (Fig. 2); the same behavior was observed following exposure to low pH (data not shown). We conclude that green and red luminescence of AO can be used in microscopic studies of DNA denaturation in nuclei of fixed cells, provided the excitation intensity is low to minimize photobleaching (17). Moreover, the metachromatic properties of AO can potentially be used to quantitate the effects of intense illumination on relative amounts of ds and ss DNA, if the appropriate corrections for photobleaching are made (see further).

AO as a photosensitiser and probe for detecting DNA denaturation in situ

We aimed to demonstrate that DNA can be denatured in fixed cells, when exciting light interacts with a luminescent intercalator. We first studied light-induced denaturation (photodenaturation) of DNA under conditions where AO acted both as a photosensitizer and probe.

When AO bound to DNA is illuminated repeatedly with blue light in a scanning confocal microscope, both intercalated and stacked forms are photobleached and emissions fall. If DNA is denatured at the same time, and the amount of dsDNA decreases while ssDNA increases, green emission (due to AO bound to dsDNA)

should fall, and red emission (due to AO stacked on ssDNA) should increase. In other words, the influence of photodenaturation and photobleaching is additive in the green but subtractive in the red (Fig. 3).

In order to analyze photodenaturation quantitatively, we investigated the kinetics of the changes in green and red luminescence. Since oxygen is likely to be involved in photobleaching of AO, and could influence denaturation, we performed the analyses both under air and anoxia. Fixed cells were stained with AO and scanned repeatedly using a confocal microscope. Green and red luminescences were imaged simultaneously. Absolute rates of intensity loss were analyzed as a function of initial pixel intensity (with pixels grouped in brightness classes ranging from the brightest to the darkest) and excitation flux, as described in Materials and Methods.

Illumination of AO bound to dsDNA led to a loss of intensity of luminescence of the monomeric (green) form of the dye, both in the presence (Fig. 4A,C) and absence (Fig. 4B,D) of oxygen. The process did not follow mono-exponential kinetics, but signal decay curves could be accurately fitted using a sum of two exponents (see Materials and Methods). The two respective exponential coefficients differed by an order of magnitude (for each brightness class). These slow and fast components were analysed as follows.

Loss of fluorescence of monomeric AO – the fast component

The absolute rates of signal loss were calculated as described in Materials and Methods. In aerated samples, the absolute rates of the fast component of the loss of green fluorescence increased linearly with initial pixel brightness (Fig. 5A). However, these rates did not depend on excitation flux, indicating that the fast processes leading to signal loss were not saturated. Correspondingly, the apparent order of these reactions was approximately 1 (0.96 ± 0.05, average $r^2 \approx 0.97$, calculated from the graph in Fig. 5E, left panel).

In argon, the absolute rates of the fast component of signal loss were also proportional to initial pixel brightness (Fig. 5B). The slight deviation from linearity was within experimental error. However, the rates of loss decreased with increasing flux of excitation light (Fig. 5B). Consequently, the apparent order of reactions was lower than 1 (average 0.70 $\pm$ 0.08, average $r^2 \approx 0.87$, calculated from Fig 5F, left panel). This indicates that the processes responsible for the fast component of signal loss were saturated at high and moderate light intensities in argon, but not in air. Anoxia suppressed the fast component of fluorescence loss at high and moderate fluxes of excitation (Fig. 5B and 5G). Therefore, oxygen-dependent reactions may contribute significantly to the fast component.

Loss of fluorescence of monomeric AO – the slow component

In aerated samples, the absolute rates of the slow component of fluorescence loss increased linearly with initial pixel brightness (Fig. 5C). However, these rates decreased with increasing flux of excitation light. Thus, the apparent order of reactions leading to a loss of fluorescence was below 1 (0.42 $\pm$ 0.10, average $r^2 \approx 0.91$, calculated from the graph in Fig. 5E, right panel).

The kinetics of fluorescence loss under anoxic conditions were similar (Fig. 5D). The apparent order of reactions responsible for the slow component of fluorescence loss was again below 1 (average 0.45 $\pm$ 0.10; average $r^2 \approx 0.88$, calculated from Fig. 5F, right panel). This dependence indicates that saturation of the slow component of fluorescence loss occurred at high photon flux of excitation light, in oxygen as well as in and argon. The absolute rates of the loss of fluorescence in the slow component were lower in the absence than in the presence of oxygen, for low and intermediate fluxes of excitation light (Fig. 5G); however they were equal at high photon flux.

We conclude that the slow and fast components are affected by oxygen and the flux of excitation light in different ways, presumably because the chemical nature of underlying reactions is different. We postulate that the slow component of

signal loss is due to photobleaching of AO monomers, while the fast one arises from an AO-sensitised denaturation of dsDNA with a subsequent reduction in intercalative binding. This hypothesis is substantiated in the sections below.

Changes of luminescence of stacked AO

Nucleoli are rich in RNA, but contain very little DNA. Prior to illumination, nucleoli of AO-stained cells fluoresced in the red as the dye was bound mainly to RNA (as a stacked form); the nucleoplasm contributed little to the overall red signal. During illumination the change of red luminescence was biphasic (Fig. 6A-D). It decreased first (which we attribute to photobleaching) and then increased (which we suggest is due to DNA denaturation). The increase becomes evident as the dose accumulates. These two phases (i.e. a loss followed by an increase) are detectable both in the presence and absence of oxygen (Fig. 6A,B). Analysis of the primary images shows that red luminescence appears in the areas originally giving green fluorescence (Fig. 7). This observation is consistent with the postulated photodenaturation of DNA.

As photobleaching occurs in parallel with denaturation (and an increase of red luminescence) the kinetics of AO photobleaching could not be determined accurately. It was possible, however, to estimate the absolute rates of photobleaching based on data collected in the initial phase of illumination, when there is little denaturation. In the presence of oxygen, the absolute photobleaching rates increased linearly with initial pixel brightness but decreased as the flux increased (Fig. 6E). Consequently, the apparent order of photobleaching reactions was lower than 1 (0.7 ± 0.05; average $r^2 \approx 0.98$, calculated from Fig. 6G). In the absence of oxygen the absolute photobleaching rates were also linear functions of pixel brightness however they did not depend on flux (Fig. 6F). Consequently, the average apparent order of photobleaching reactions was close to 1 (0.95 ± 0.05, average $r^2 \approx 0.99$, calculated from Fig. 6H). This indicates that increasing flux saturates photobleaching in the presence of oxygen but not in argon. Anoxia suppressed photobleaching of the aggregate AO

form over the whole range of fluxes with the effect being most clearly pronounced at low intensities (Fig 6I).

In order to estimate rates of the light-induced denaturation of DNA, changes in intensity of red luminescence were measured exclusively in areas of nuclei occupied initially by monomeric AO (i.e. in the green). Two phases were again observed (after correcting for intensity loss due to breakdown of stacks and AO diffusing into the solution, and photobleaching of AO aggregates, see Materials and Methods) (Fig. 8A-D); the intensity of luminescence of AO stacks was initially constant, but then increased as DNA became denatured. As before, initial rates of signal loss were determined (Fig. 8E,F). In the presence of oxygen, the rates of increase of red luminescence were proportional to the initial brightness (i.e. initial intensity of green fluorescence) and independent of flux (Fig. 8E). Hence, the average apparent order of photodenaturation was close to 1 (0.87 $\pm$ 0.10, average $r^2 \approx 0.97$, calculated from Fig. 8G).

Under argon, patterns were roughly similar but rates decreased with increasing flux (Fig. 8F). The apparent order of photodenaturation was lower than 1 (0.52 $\pm$ 0.12, average $r^2 \approx 0.94$, calculated from Fig. 8H) while anoxia decreased rates only at the highest flux (Fig. 8I).

The recovery of red luminescence and the fast component of monomeric AO signal loss exhibited a similar dependence on photon flux and oxygen presence. This reinforces the conclusion that the fast phase of the loss of green fluorescence and the recovery of red luminescence are related and arise from DNA photodenaturation.

Influence of focal depth on photobleaching and photodenaturation

Since the excitation light flux is a function of the distance from the focal plane one may hypothesize that changes of AO luminescence in cell nuclei depend on this parameter as well. Thus, distributions of the monomeric and aggregate AO

luminescence before and after intense illumination of one optical section (using bleaching beam, 3.33 W/cm^2, 4.4 kJ/ cm^2) were compared (Fig. 9). One may note that while monomeric AO fluorescence decreased, the aggregate AO luminescence increased, as described in the previous sections. Furthermore, these changes were uniform throughout nuclei indicating that excitation light flux did not influence significantly the absolute photobleaching and photodenaturation rates. The thickness of the nuclei (5.0 – 7.5 μm) was small enough so that all horizontal (xy) optical sections in nuclei received a similar total dose of excitation light.

Photodenaturation with EB and Hoechst

In the experiments described above, AO served both as photosensitiser and a probe reporting about denaturation. In order to establish if photodenaturation can also be caused by other DNA stains, similar experiments were carried out using EB (an intercalator) and Hoechst 33342 (a minor groove binder) as potential sensitizers. Illumination lead to denaturation of DNA stained with EB, as demonstrated by subsequent staining with AO (Fig. 10). However, no increase of the aggregate AO luminescence was detectable in nuclei stained with Hoechst, indicating that this dye was not capable of catalyzing DNA photodenaturation under our experimental conditions.

Discussion

We interpret the behaviour of green and red luminescence of AO bound to nuclear DNA during illumination as evidence of photosensitised denaturation of the nucleic acid. This notion is based on knowledge of the metachromatic properties of AO bound to ss and ds nucleic acids, and on an analysis of the changes in luminescence that occur during scanning in a confocal microscope.

The increase of red luminescence occurs in areas initially occupied by green fluorescence. Any role of DNA repair or some unknown physiological processes leading to DNA denaturation can also be ruled out, since the phenomenon was observed in fixed cells. The increase of red luminescence is not an artifact resulting from correction for the diffusion of the aggregate form to the incubation medium, as it was evident even when the correction was not applied (Fig. 7, Fig. 9). The loss of monomeric AO fluorescence comprised the fast and the slow components. One may postulate that these were due to the difference in excitation light flux between the center and the horizontal borders of the optical section. However, while the difference in flux was only 4.92, the respective exponential coefficients (eq. 1) of the fast components were an order of magnitude higher in comparison with the slow components. Furthermore, the slow and fast components exhibit a difference in apparent reaction orders (resulting from the dependence on the excitation light flux) and a different pattern of dependence on oxygen concentration. Consequently, it seems likely that these two components represent different reactions. The fact that the loss of the monomeric AO fluorescence was uniform in the whole volume of a nucleus illuminated intensely only in one optical section (Fig. 9) reinforces this notion. The rates of monomeric AO fluorescence loss (fast component) and the rates of photodenaturation present a similar pattern of dependence on excitation light flux and oxygen. It should also be emphasized that intensity loss of red luminescence follows a different pattern (compare Fig 6I and 8I). These observations lead us to postulate that the increase in the red/green luminescence ratio in cell nuclei results from the photosensitized transition of dsDNA to ssDNA (i.e. photodenaturation).

The metachromatic properties of AO have been used to study apoptosis (13,18, 19), asses sperm quality (20, 21, 22) and investigate the mechanisms of action of anti-tumor drugs (23). Differences in susceptibility towards DNA denaturation were exploited to differentiate between normal and tumor cells and separate phases of cell cycle (6, 12, 24). These studies relied on global denaturation of

DNA, induced using high temperature (4) and alkali or acids (5, 6). Here we report that DNA may be denatured in photosensitised reaction. This phenomenon makes it feasible to study the susceptibility of selected local regions of DNA towards denaturation. The possible photodenaturation of DNA was suggested previously by others (25, 26, 27). It has been suggested that denaturation of DNA might occur as a result of photosensitised oxidation of guanine in fixed cells and isolated DNA (27, 28, 29). However, these authors did not demonstrate that the light-induced changes in chromatographic DNA mobility (27) or staining pattern of mitotic chromosomes (25, 26), that they observed, were due to a transition between ds and ss DNA.

It has been demonstrated that the degree of condensation affects susceptibility of chromatin to denaturation (5, 6). In agreement with these previous observations, our preliminary data indicate that condensed chromatin in metaphase undergoes photodenaturation more rapidly than relaxed chromatin in interphase. However, due to a low spatial resolution of the images recorded in this study the differences in denaturability between eu- and heterochromatin within single fibroblast nuclei were not detectable.

The data available so far do not reveal the mechanism of DNA photodenaturation. However, it should be noted that excited AO may induce several kinds of phototoxic damage in cells (30, 31, 32). It was demonstrated that excitation of AO bound to ds nucleic acids can result in production of reactive oxygen species (33, 34). Furthermore, reactions of several acridine derivatives with the sugar backbone and bases have been reported (35, 36). One should note again that the onset of the increase of the red luminescence is delayed with respect to the photobleaching of the monomeric form of AO. The delay seems to be constant regardless of excitation flux and is unlikely to arise from the time needed to form stacks (as this process is much faster). Thus, it seems plausible that the photosensitized reaction of AO does not lead directly to breakage of hydrogen bonds in DNA. Since this effect is observed even in the absence of

oxygen one may speculate that monomer of AO reacts directly with deoxyribose (rather than the base) to form a single strand break (35). If true, photodenaturation then results from an unwinding of DNA probably driven by torsional stress (9, 4). The fact that the photodenaturation can be caused by another DNA intercalator, EB, but not a minor groove binder Hoechst 33342 (Fig. 10), is in agreement with this notion. It has been demonstrated that susceptibility towards denaturation correlates with the amount of DNA strand breaks (37, 38), which is consistent with this hypothesis.

We feel that the results presented in this paper have several practical implications. These may be summarized as follows:

- Illumination of fluorescently labeled double stranded nucleic acids may lead to modification of their spatial structure. Thus phenomenon may limit applicability of fluorescent labeling in studies of nucleic acids,
- As modern scanning microscopes allow selected regions of cells to be illuminated, photodenaturation can be applied under physiological conditions to study DNA repair and chromatin remodeling,
- It seems possible that photodenaturation and its subsequent detection may depend on the concentration of a free dye and the mass ratio of the dye to nucleic acids (4, 5). These factors have to be accounted for to obtain reproducible and meaningful results,
- Some of the DNA-binding drugs used in photodynamic therapies (35) may exert their action through photodenaturation of nucleic acids and a subsequent modification of higher-order chromatin structures.

References

1 Blackburn, G.M., J.M. Gait (1996) *Nucleic acids in chemistry and biology*, Oxford University Press, Oxford, New York, Tokyo,

2 Saenger, W. (1984) *Principles of Nucleic Acid Structure*, Springer - Verlag, New York, Berlin, Heidelberg, Tokyo,

3 Sinha, R. P. and D. P. Hader, (2002) Uv-induced dna damage and repair: a review. *Photochemical & Photobiological Sciences* 1, 225-36.

4 Zelenin, A. V. (1993) Acridine orange as a probe for molecular and cell biology in: *Luminescent Probes for Biological Activity* (Edited by: W. T. Mason) pp. 83-99 Academic Press, New York.

5 Darzynkiewicz, Z., (1990) Acid-induced denaturation of dna in situ as a probe of chromatin structure. *Methods in Cell Biology.* 33, 337-52 .

6 Dobrucki, J. and Z. Darzynkiewicz, (2001) Chromatin condensation and sensitivity of DNA in situ to denaturation during cell cycle and apoptosis--a confocal microscopy study. *Micron* 32, 645-52.

7 Schwarzacher, T., J.S. Heslop-Harrison (2000) *Practical in situ hybridisation.*, Bios Scientific Publishers, Oxford

8 Traganos, F., Z. Darzyndiewicz, T. Sharpless, and M. R. Melamed, (1975) Denaturation of deoxyribonucleic acid in situ effect of formaldehyde. *Journal of Histochemistry & Cytochemistry* 23, 431-8.

9 Darzynkiewicz, Z.,J. Kapuscinski (1990) Acridine Orange: A Versatile Probe of Nucleic Acids and Other Cell Constituents in: *Flow Cytometry and Sorting* (Edited by: M. R. Melamed, T. Lindmo, M. R. Mendelsohn) pp. 291-314 Wiley-Liss Inc., New York.

10 Dolbeare, F., H. Gratzner, M. G. Pallavicini, and J. W. Grey, (1983) Flow cytometric measurement of total dna content and incorporated bromodeoxyuridine. *Proceedings of the National Academy of Sciences of the United States of America* 80, 5573-7.

11 Darzynkiewicz, Z., (1990) Differential staining of DNA and RNA in intact

cells and isolated cell nuclei with acridine orange. *Methods in Cell Biology.* 33, 285-98.

12 Darzynkiewicz, Z. (1990) Probing Nuclear Chromatin by Flow Cytometry in: *Flow Cytometry and Sorting* (Edited by: M. R. Melamed, T. Lindmo, M. R. Mendelsohn) pp. 315-340 Wiley-Liss Inc., New York.

13 Lecoeur, H., (2002) Nuclear apoptosis detection by flow cytometry: influence of endogenous endonucleases. *Experimental Cell Research* 277, 1-14.

14 Morgan, T. L., D. J. Yang, D. G. Fry, P. J. Hurlin, S. K. Kohler, V. M. Maher, and J. J. McCormick, (1991) Characteristics of an infinite life span diploid human fibroblast cell strain and a near-diploid strain arising from a clone of cells expressing a transfected v-myc oncogene. *Experimental Cell Research* 197, 125-36.

15 Tossi, A. B. and J. M. Kelly, (1989) A study of some polypyridylruthenium(II) complexes as DNA binders and photocleavage reagents. *Photochemistry & Photobiology* 49, 545-56.

16 Patterson, G. H., S. M. Knobel, W. D. Sharif, S. R. Kain, and D. W. Piston, (1997) Use of the green fluorescent protein and its mutants in quantitative fluorescence microscopy. *Biophysical Journal* 73, 2782-90.

17 Bernas, T., M. Zarebski, P.R. Cook, J.W. Dobrucki, (2004) Minimizing photobleaching during confocal microscopy of fluorescent probes bound to chromatin: role of anoxia and photon flux. *Journal of Microscopy* 215, 281-296.

18 Darzynkiewicz, Z., S. Bruno, G. Del Bino, W. Gorczyca, M. A. Hotz, P. Lassota , and F. Traganos, (1992) Features of apoptotic cells measured by flow cytometry. *Cytometry* 13, 795-808.

19 Hotz, M. A., J. Gong, F. Traganos, and Z. Darzynkiewicz, (1994) Flow

cytometric detection of apoptosis: comparison of the assays of in situ DNA degradation and chromatin changes. *Cytometry* 15, 237-44.

20 Ballachey, B. E., D. P. Evenson, and R. G. Saacke, (1988) The sperm chromatin structure assay. Relationship with alternate tests of semen quality and heterospermic performance of bulls. *Journal of Andrology* 9, 109-15.

21 Erenpreiss, J., J. Bars, V. Lipatnikova, J. Erenpreisa, and J. Zalkalns, (2001) Comparative study of cytochemical tests for sperm chromatin integrity. *Journal of Andrology* 22 , 45-53.

22 Evenson, D. P., L. K. Jost, D. Marshall, M. J. Zinaman, E. Clegg, K. Purvis, P. de Angelisand O. P. Claussen, (1999) Utility of the sperm chromatin structure assay as a diagnostic and prognostic tool in the human fertility clinic. *Human Reproduction* 14, 1039-49.

23 Baisch, H., H. Bollmann, and S. Bornkessel, (1999) Degradation of apoptotic cells and fragments in hl-60 suspension cultures after induction of apoptosis by camptothecin and ethanol. *Cell Proliferation* 32, 303-19.

24 Bretton, P. R., Z. Darzynkiewicz, E. Henry, M. Kimmel, W. R. Fair, and M. R. Melamed, (1990) DNA in situ sensitivity to denaturation in bladder cancer and its correlation with tumor stage. *Cancer Research* 50, 7912-4.

25 Cerdan, E., J. Pasantes, J. Mendez, and V. Goyanes, (1988) Changes in metaphasic chromosomal ultrastructure caused by denaturing treatments. *Cytobios* 55, 167-70.

26 Cerdan, M. E., J. Pasantes, A. Martinez-Lage, and J. Mendez, (1989) Denaturing effect of acridine orange and adriamycin. *Cytobios* 60, 151-5.

27 Dhar, A. and U. Chaudhuri, (1974) The intermediate in the photodegradation of DNA in the presence of acridine orange. *Archives of Biochemistry & Biophysics* 162, 310-2.

28 Ferruchhi, L. and A. T. Sumner, (1984) Further evidence for the DNA base specificity of light-induced banding. *Histochemical Journal* 16, 521-8.

29 Mezzanotte, R., L. Ferrucci, A. Marchi, and U. Bianchi, (1982) The longitudinal differentiation produced by photo-oxidation and acridine-orange staining in eukaryote chromosomes: role and involvement of DNA base composition. *Cytogenetics & Cell Genetics* 33, 277-84.

30 Hashiguchi, S., K. Kusuzaki, H. Murata, H. Takeshita, M. Hashiba, T. Nishimura, T. Ashihara, and Y. Hirasawa, (2002) Acridine orange excited by low-dose radiation has a strong cytocidal effect on mouse osteosarcoma. *Oncology* 62, 85-93.

31 Martin, J. P. and N. Logsdon, (1987) Oxygen radicals mediate cell inactivation by acridine dyes, fluorescein, and lucifer yellow. *Photochemistry & Photobiology* 46, 45-53.

32 Zdolsek, J. M., G. M. Olsson, and U. T. Brunk, (1990) Photooxidative damage to lysosomes of cultured macrophages by acridine orange. *Photochemistry & Photobiology* 51, 67-76.

33 Amagasa, J., (1986) Binding of acridine orange to transfer RNA and photodynamic inactivation. *Journal of Radiation Reserach* 27, 325-338.

34 Amagasa, J., (1986) Mechanisms of photodynamic inactivation of acridine orange-sensitized transfer RNA: Participation of singlet oxygen and base damage leading to inactivation. *Journal of Radiation Reserach* 27, 339-351.

35 Armitage, B., (1998) Photocleavage of Nucleic Acids. *Chemical Review* 98, 1171-1200.

36 Kurbanyan, K., K. L. Nguyen, P. To, E. V. Rivas, A. M. Lueras, C. Kosinski, M. Steryo, A. Gonzalez, D. A. Mah, and E. D. Stemp, (2003) DNA-protein cross-linking via guanine oxidation: dependence upon protein and photosensitizer. *Biochemistry* 42, 10269-81.

37 Gorczyca, W., F. Traganos, H. Jesionowska, and Z. Darzynkiewicz, (1993) Presence of DNA strand breaks and increased sensitivity of DNA in situ to denaturation in abnormal human sperm cells: analogy to apoptosis of somatic cells. *Experimental Cell Research* 207, 202-5.

38 Rydberg, B., (1984) Detection of DAN strand breaks in single cells using flow cytometry. *International Journal of Radiation Biology & Related Studies in Physics, Chemistry & Medicine* 46, 521-7.

Acknowledgements

This work was supported by The Wellcome Trust (IRDA grant to PRC, JWD) and Polish State Committee for Scientific Research (JDD, grant 0278/P04/2001/21). The confocal microscope was funded by the Foundation for Polish-German Cooperation in Warsaw. We acknowledge excellent technical assistance by Barbara Czuba-Pelech, Eng. In preparing this work we benefited from helpful discussion with Prof. J.Maluszynska (TB).

Figure legends

Fig 1.

Schematic representation of different modes of AO binding to nucleic acids. At a concentration of 5-10 μg/ml the dye monomers intercalate to ds nucleic acids and form aggregates on ss nucleic acids. As a concencentration of AO increases, the dye, which binds to ds nucleic acids begins to form aggregates by ionic interactions.

Fig. 2.

Denaturation of DNA in nuclei of fixed cells by formamide. The average intensity (arbitrary units; au) of the red and green AO luminescence in cell nuclei (bottom axis) as well as the red/green ratio (top axis) is shown. The intensities were measured in the cell areas occupied initially by ds but not ss nucleic acids (see Materials and Methods). Treatment with formamide ('form') resulted in a decrease of green luminescence (AO monomers at dsDNA) and concomitant slight increase of red luminescence (AO stacks on ssDNA), i.e. red/green ratio increased in comparison with control ('ctrl'). Error bars - 95% confidence intervals. Photobleaching of green fluorescence was negligible during data collection, but red emission bleached rapidly (by approx. 20 %). This loss obfuscated the increase of red luminescence arising from DNA denaturation.

Fig. 3.

A schematic representation of influence of AO photobleaching and DNA photodenaturation on luminescence of AO in illuminated nuclei of fixed cells. When AO-stained cells are repeatedly illuminated with blue light, photobleaching of the monomeric (green) and stacked (red) form of AO occurs and is manifested by a decrease of green and red luminescence. Repeated illuminations also cause DNA photodenaturation. This process leads to further loss of green luminescence, as a result of diminishing number of binding sites for intercalation of the monomeric AO. At the same time the red luminescence increases as new binding sites for a stacked AO are formed on denatured DNA. The net result of continuous illumination of DNA decorated with AO is a continuous loss of green luminescence, and an initial loss followed by a moderate increase of red luminescence. The kinetics of net changes of red luminescence depends on the relative contributions of photobleaching and photodenaturation.

Fig. 4.

Kinetics of the loss of fluorescence of the monomeric form of dsDNA-bound AO during illumination in air (A,C) or argon (B,D). The average intensity (arbitrary units; au) of pixels of different initial brightness is plotted relative to the

accumulated dose of light. The flux of the incident light is indicated. In each pair of panels, curves 1 and 11, 2 and 12, and so on were obtained in air and argon, respectively; this convention is used in the equivalent pairs of panels in other Figs.

A. Signal loss follows non-monoexponential kinetics. Curves for pixels of only 3 (bright, intermediate, dim) out of 25 brightness classes are shown for clarity. Mean of 5 experiments.

B. Argon lessens signal loss, both the slow and fast component. Curves 1-3 from (A) are included for comparison with their counterparts (i.e., 11-13) in argon.

C. Effect of 3 different fluxes on signal loss. Only bright (curves 4-6) and dim pixels (curves 7-9) are shown for clarity.

D. The rates of luminescence loss decrease under anoxia.

Fig. 5.

Analysis of kinetics of fluorescence loss of the monomeric form of dsDNA-bound AO in air (A, C, E) and argon (B,D,F).

A,B. Absolute rates of the fast component of fluorescence loss, as a function of initial pixel brightness. Increasing light intensity does not affect fluorescence loss rate in air, but brings about a decrease in argon. This indicates that saturation of the process of signal loss occurs under argon but not under air. Error bars: 95% confidence intervals.

C,D. As A,B, for slow-phase fluorescence loss. Saturation occurs to a similar extent in air and under argon.

E,F. Rates of fluorescence loss (bright pixels only) for the fast and slow components (graphs on left and right in each panel, respectively). The order of the fast component of fluorescence loss reactions (see Materials and Methods) is approximately 1 in air (0.96) and below 1 in argon (0.70). The order of the slow component is well below 1 under air (0.42) and argon (0.45).

G. Ratios between absolute signal loss rates in argon and air, for the fast and slow component of the signal loss. Error bars: 95% confidence intervals. Ratios of signal loss decrease with growing photon flux for the slow phase, but increase

for the fast phase. This observation suggests that the mechanisms of fast and slow processes causing a loss of green fluorescence are different.

Fig. 6.

The effect of illumination on luminescence intensity of the aggregate form of AO in air (A, C, E) or argon (B, D, F) in nuclei of fixed cells. The general approach was as described in Fig. 3. Changes of red luminescence of AO are a net consequence of DNA denaturation (leading to signal increase) and photobleaching (resulting in signal loss) – see text for further description.

A. An initial loss of red luminescence is followed by recovery. Curves for pixels of only 3 (bright, intermediate, dim) out of 25 pixel brightness classes are shown for clarity. Means of 5 experiments.

B. Argon inhibits the initial loss of luminescence but has only slight effect on the subsequent increase of the signal. Curves 1-3 from (A) are included for comparison with their counterparts (i.e., 101 -103) in argon.

C. Effect of 3 different photon fluxes on the kinetics of luminescence changes. Effects on only bright (curves 4-6) and dim pixels (curves 7-9) are shown for clarity. A recovery of red luminescence is prominent at low photon flux; at a high photon flux no recovery occurs.

D. Removal of oxygen slows down the initial signal loss.

E,F. Absolute rates of luminescence loss as a function of initial pixel brightness. Increasing photon flux brings about a decrease of signal loss rate in air; there is no effect in argon. Saturation of the process of signal loss occurs under air but not under argon. Error bars: 95% confidence intervals.

G,H. Bleaching rates for bright pixels. Reaction order is lower than 1 in air (0.7) and close to 1 in argon (0.95).

I. Ratio of the absolute rates of signal loss in argon and air. At a low photon flux oxygen-dependent reactions dominate; the contribution of reactions not involving oxygen is greater at high photon flux. Error bars: 95% confidence intervals.

Fig. 7.

Image of fixed MSU 1.1 cells stained with AO, showing green fluorescence of DNA in nuclei and red luminescence of RNA in nucleoli and cytoplasm (this image was created using a low-intensity laser beam). A fragment of the field of view (the right-bottom corner, marked with a blue line) was illuminated (zoom 2.0) with a dose of light, which caused photobleaching of AO and photodenaturation of DNA. These two processes resulted in a decrease of green fluorescence of monomeric AO in regions of nuclei occupied by DNA, while red luminescence of aggregate AO increased in these regions due to DNA photodenaturation. Photobleaching resulted in a net decrease of red luminescence of RNA-bound AO in cytoplasm and nucleoli (no DNA and no DNA photodenaturation). Bar – 10 μm.

Fig. 8.

The increase of the luminescence intensity of the aggregate form of AO in the areas occupied initially by monomeric form of the dye, measured in air (A, C, E) or argon (B, D, F). In contrast to Fig. 5, these measurements are confined to areas of nuclei occupied initially by dsDNA only. In these regions any increase of red luminescence can be attributed to denaturation of DNA. The general approach was as described in Fig. 1.

A. Increase of luminescence is observed in bright pixels only. The onset of the increase is delayed with respect to the start of illumination. Curves for pixels of only 3 (bright, intermediate and dim) out of 25 brightness classes are shown for clarity. Means of 5 experiments.

B. Removal of oxygen does not affect the increase of luminescence in its initial phase at moderate flux of incident light. Curves 1-3 from (A) are included for comparison with their counterparts (i.e., 101 -103) in argon.

C. Effect of 3 different photon fluxes on the kinetics of luminescence changes. Effects on only bright (curves 4-6) and dim pixels (curves 7-9) are shown for clarity. Recovery of red luminescence does not depend on photon flux.

D. Removal of oxygen has no effect on recovery of red luminescence at low photon fluxes, but slows down the recovery at high flux of incident light.

E,F. Absolute rates of signal recovery (photodenaturation rates) as a function of initial pixel brightness. Increasing the flux does not affect the rates of recovery in argon, and brings about decrease of signal loss rates in air. Saturation of signal recovery occurs under air, but not under argon. Error bars: 95% confidence intervals.

G,H. Photodenaturation rates for bright pixels. Reaction order is close to 1 in air (0.87) and lower than 1 in argon (0.52).

I. Ratio of the absolute rates of signal change in argon and air. At low photon flux the rates are similar, i.e. DNA photodenaturation is not oxygen-dependent, but at higher photon fluxes reactions involving oxygen occur and their contribution increases with flux. Error bars: 95% confidence intervals.

Fig 9.

Vertical cross-sections through images of nuclei exposed to a scanning high-intensity, bleaching laser beam (3.33 W/cm2, 4.4 kJ/ cm^2), focused in one horizontal plane (arrow). Luminescence of the monomeric (A,B) and the aggregate (C,D) AO forms is shown. XZ sections through the nuclei were registered using a probing beam before (A,C) and after (B,D) bleaching of the selected plane. Position of the coverslip is indicated with the grey dashed line. A comparison of images in A and C demonstrates that the loss of luminescence was not confined to the selected illuminated plane but extended throughout the depth of the nucleus; moreover the rates of photobleaching are similar in planes at different depth.

Fig. 10. Photodenaturation of DNA, induced by Ethidium bromide (EB) or Hoechst 33342 (HOE), monitored using AO. Cells were stained with EB or HOE and a part of the field of view was exposed to light. Next, cells were stained with AO, as in previous experiments, to reveal DNA denaturation. Intensity of red and green luminescence of AO (bottom axis) and their ratio (top axis) are shown for the unilluminated (no light) and illuminated (light) nuclei. Fluorescence of EB and

HOE is not detectable under these conditions. Error bars: 95% confidence intervals.

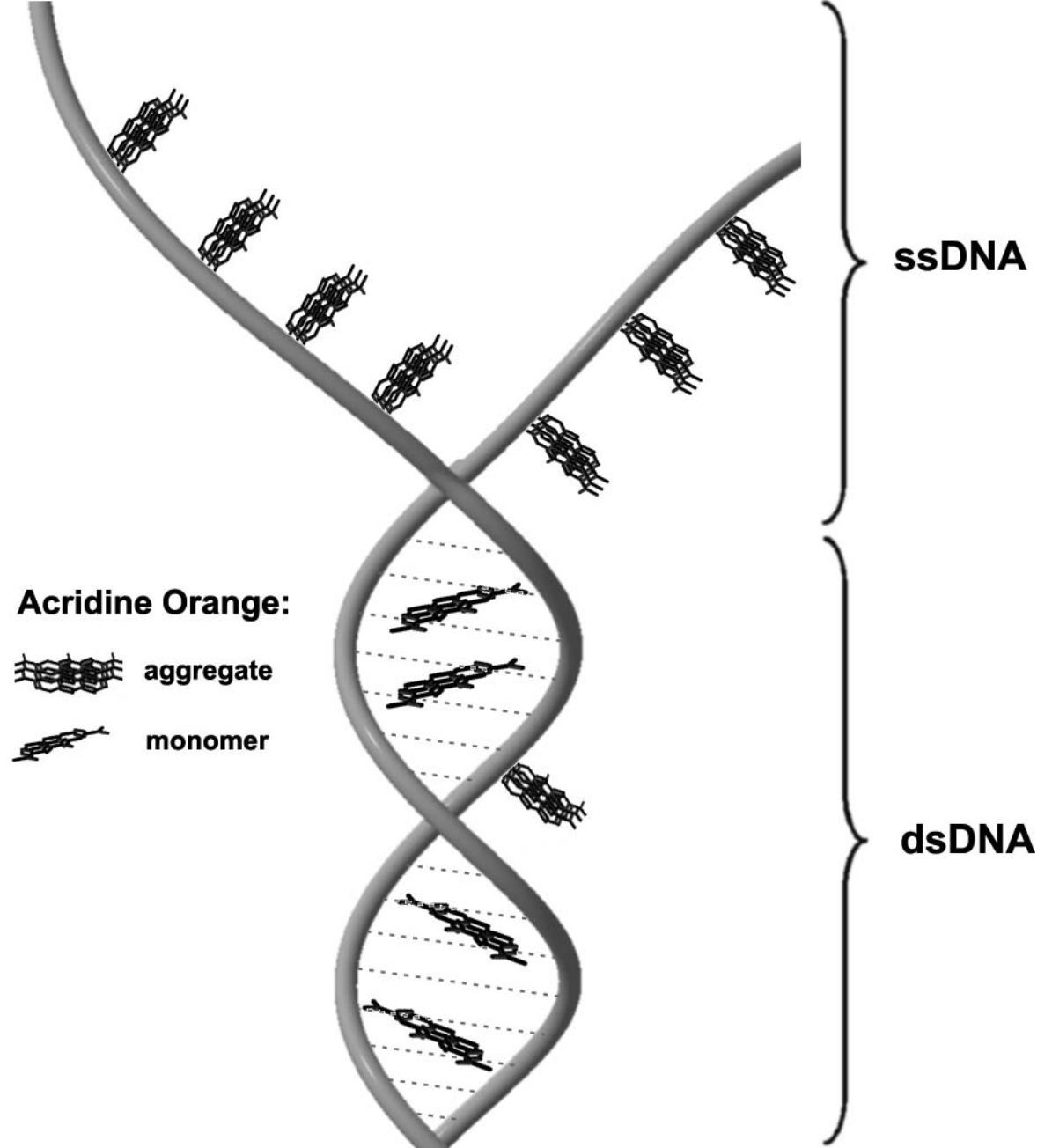
ssDNA
Acridine Orange:
aggregate
monomer
dsDNA

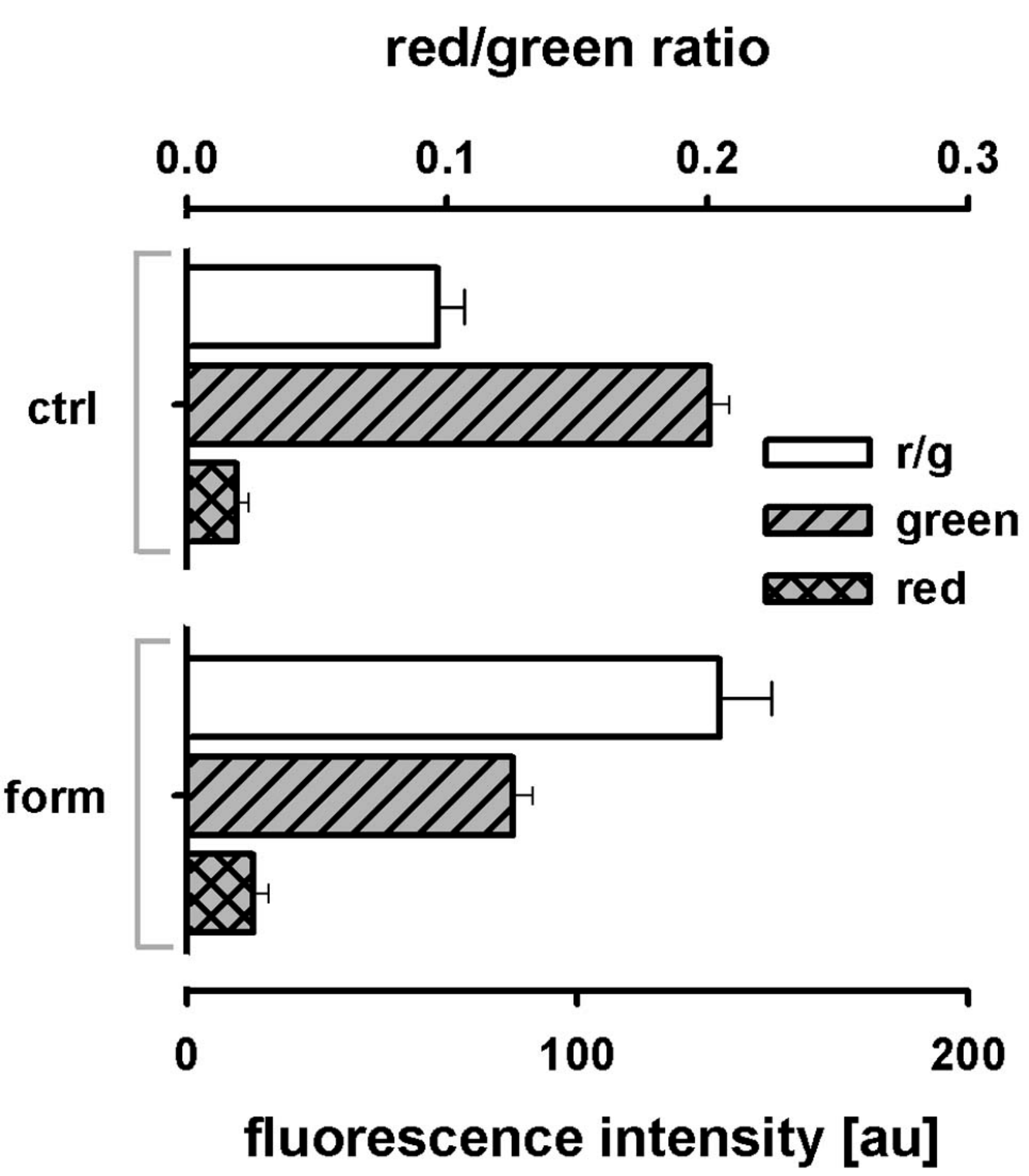
red/green ratio
0.0
0.1
0.2
0.3
ctrl
form
r/g
green
red
0
100
200
fluorescence intensity [au]

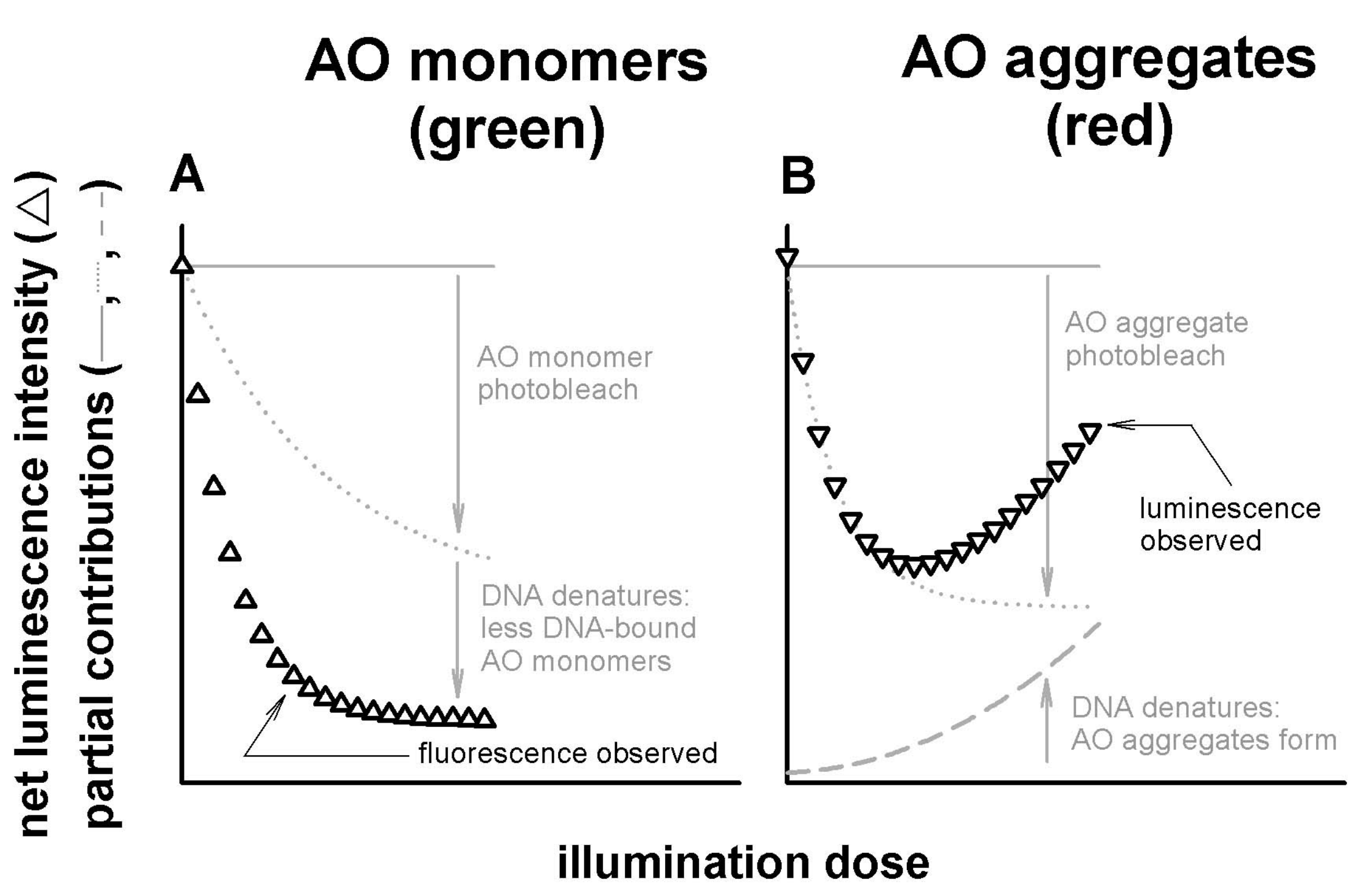
AO monomers
(green)
AO aggregates
(red)
A
B
net luminescence intensity (△)
partial contributions (——, ·····, – –)
AO monomer
photobleach
DNA denatures:
less DNA-bound
AO monomers
fluorescence observed
AO aggregate
photobleach
luminescence
observed
DNA denatures:
AO aggregates form
illumination dose

AO, green fluorescence

air

argon

A

B

C

D

scan number

0

350

700

3.33 W/cm^2

250

125

0

1 (bright)

2 (medium)

3 (dark)

11

13

1

3

2

12

4 (1.11 W/cm^2)

5 (3.33 W/cm^2)

6 (11.10 W/cm^2)

7

8

9

14

15

16

17

18

19

0

4

8

0.0

3.5

7.0

fluorescence intensity [au]

illumination dose [kJ/cm^2]

AO, green fluorescence

air

argon

A

B

C

D

signal loss rate [au]

0.00
0.15
0.30
0.06
0.12

1
2
3
4
5
6

11 (1.11 W/cm^2)
12 (3.33 W/cm^2)
13 (11.1 W/cm^2)
14
15
16

0
125
250

fluorescence intensity [au]

E

F

ln loss rate

1
-3

7
8
18

-0.5
3.5

ln flux

G

flux [W/cm^2]

11.10
3.33
1.11

fast
slow

0.0
0.5
1.0

signal loss rate ratio (anox/ox)

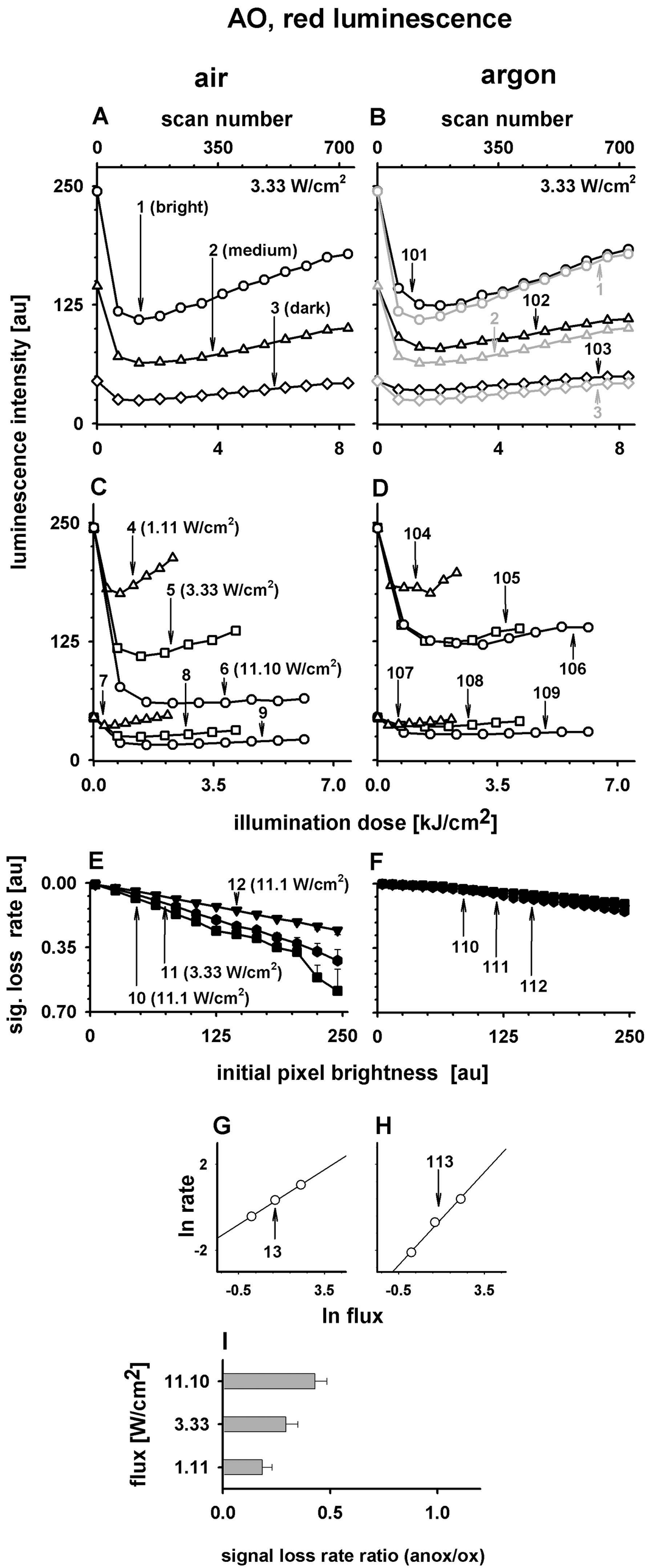
AO, red luminescence
air
argon
A
scan number
0
350
700
3.33 W/cm2
1 (bright)
2 (medium)
3 (dark)
250
125
0
4
8
B
101
102
103
1
2
3
C
4 (1.11 W/cm2)
5 (3.33 W/cm2)
6 (11.10 W/cm2)
7
8
9
D
104
105
106
107
108
109
0.0
3.5
7.0
luminescence intensity [au]
illumination dose [kJ/cm2]
E
F
12 (11.1 W/cm2)
11 (3.33 W/cm2)
10 (11.1 W/cm2)
110
111
112
0.00
0.35
0.70
sig. loss rate [au]
initial pixel brightness [au]
G
H
ln rate
2
-2
13
113
-0.5
3.5
ln flux
I
flux [W/cm2]
11.10
3.33
1.11
0.0
0.5
1.0
signal loss rate ratio (anox/ox)

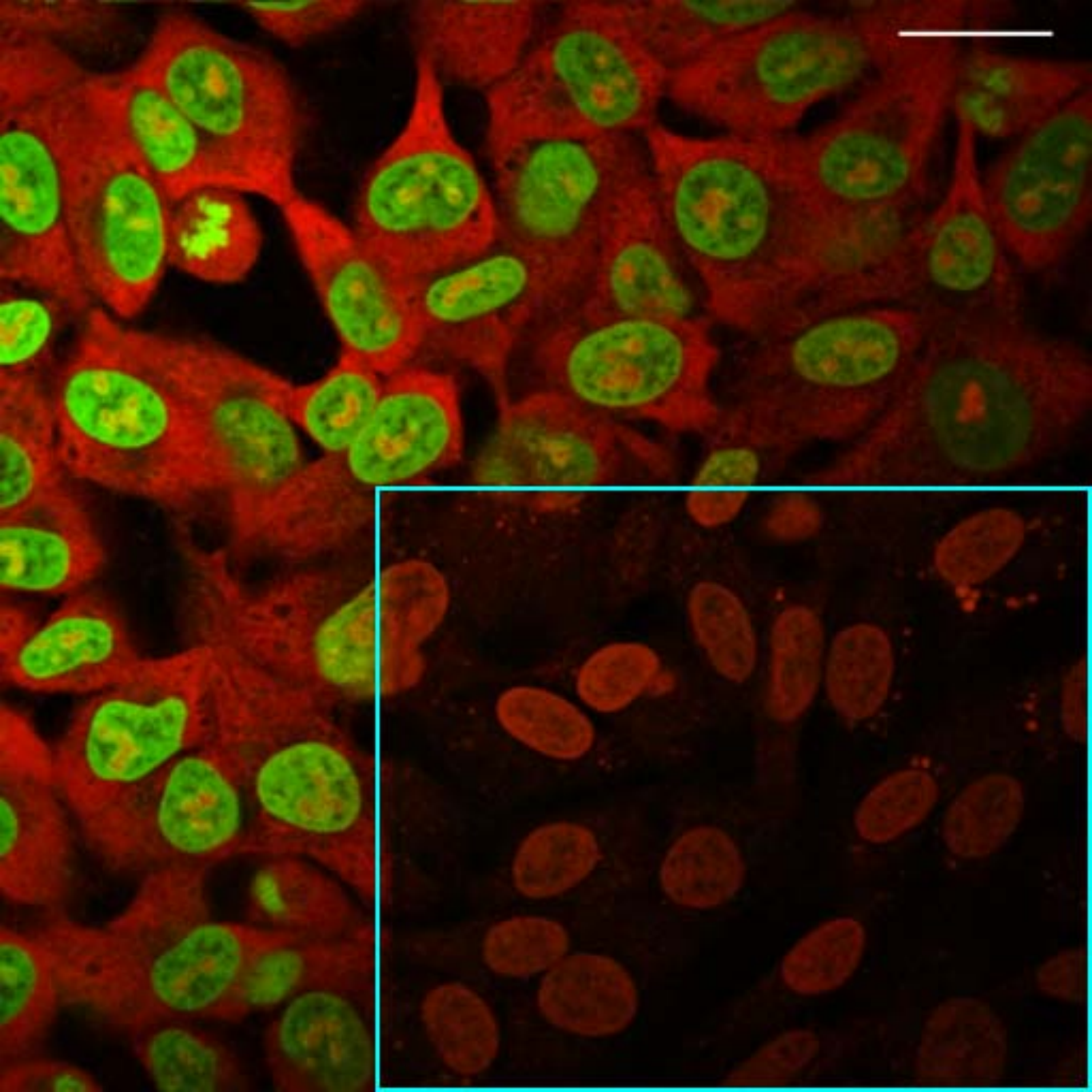

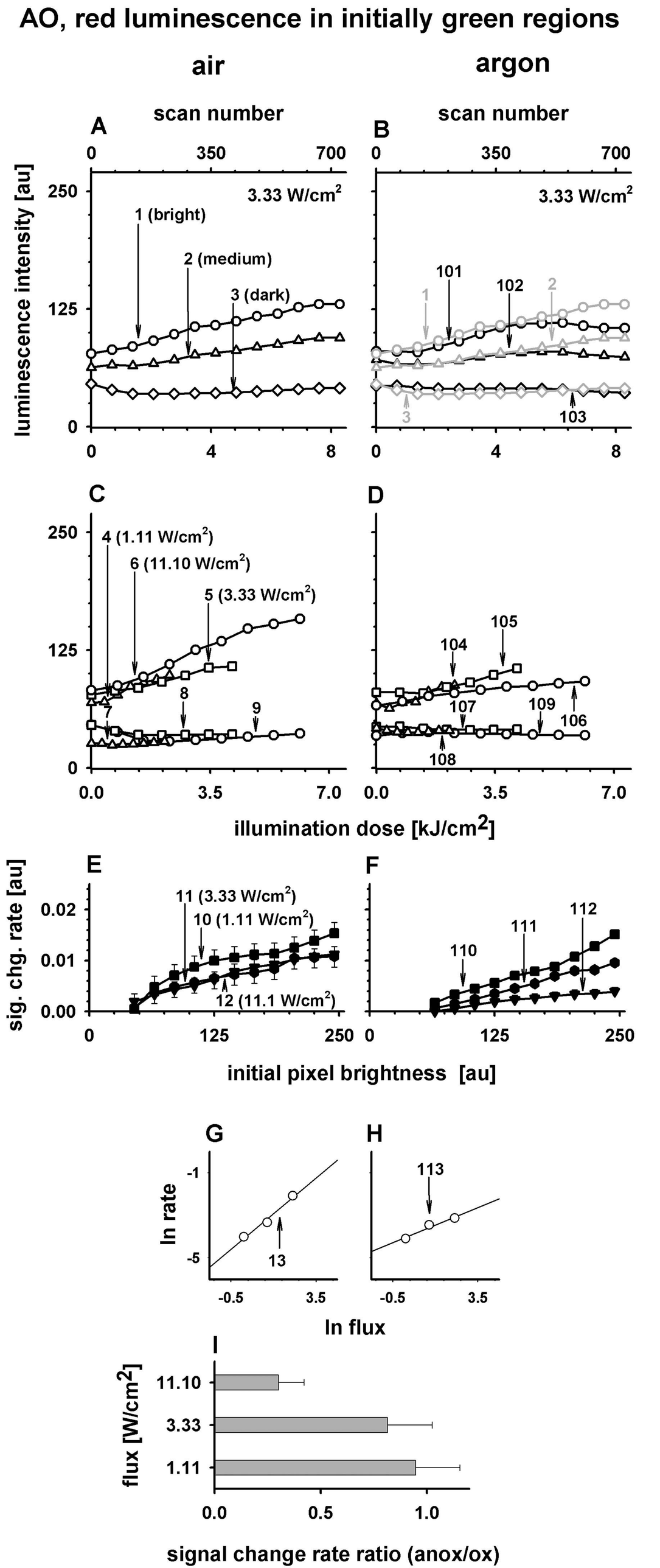
AO, red luminescence in initially green regions
air
argon
A
B
C
D
E
F
G
H
I
scan number
scan number
luminescence intensity [au]
3.33 W/cm2
1 (bright)
2 (medium)
3 (dark)
101
102
103
4 (1.11 W/cm2)
6 (11.10 W/cm2)
5 (3.33 W/cm2)
104
105
106
107
108
109
illumination dose [kJ/cm2]
sig. chg. rate [au]
11 (3.33 W/cm2)
10 (1.11 W/cm2)
12 (11.1 W/cm2)
110
111
112
initial pixel brightness [au]
ln rate
13
113
ln flux
flux [W/cm2]
11.10
3.33
1.11
signal change rate ratio (anox/ox)

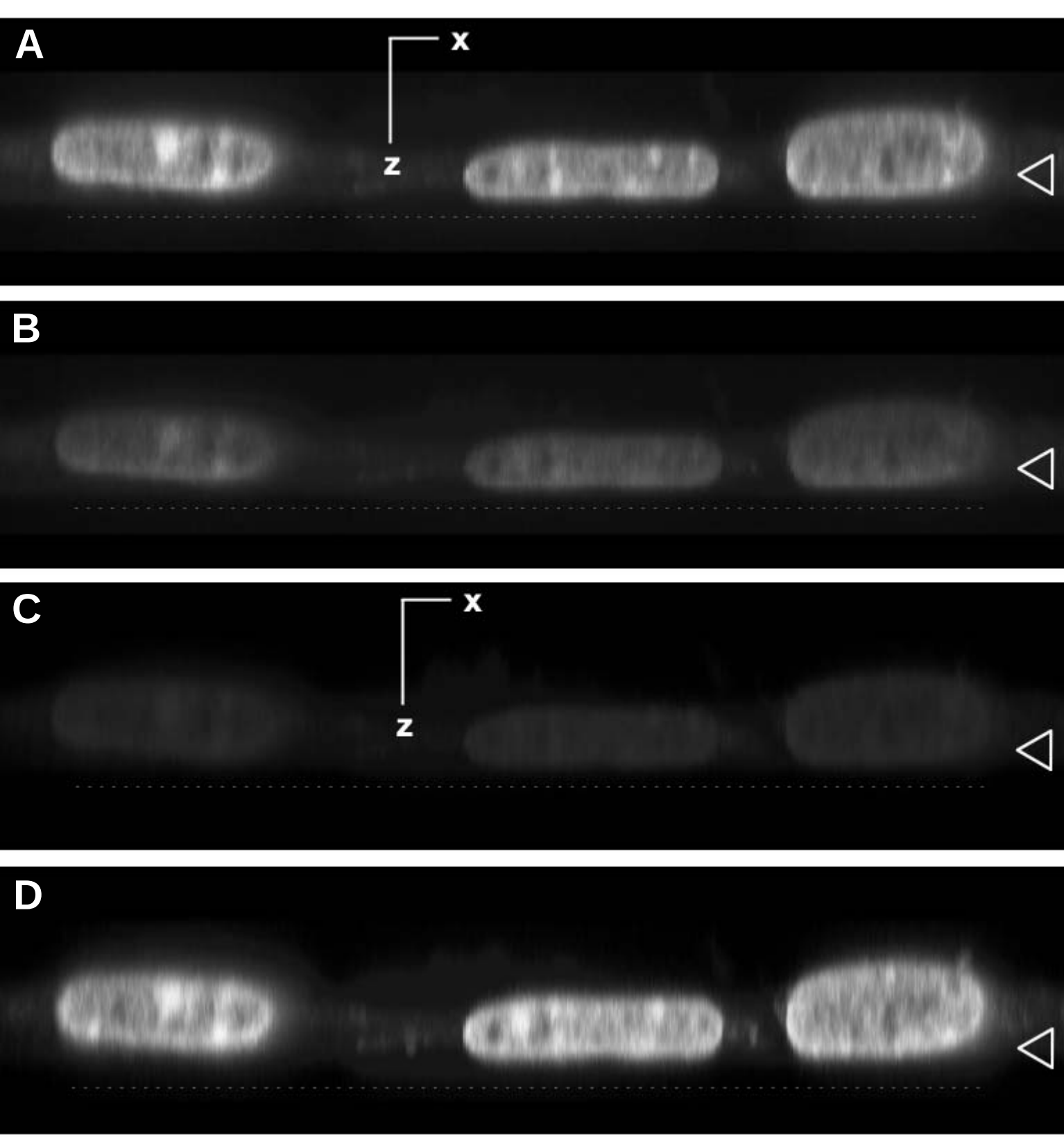
A
x
z
B
C
x
z
D

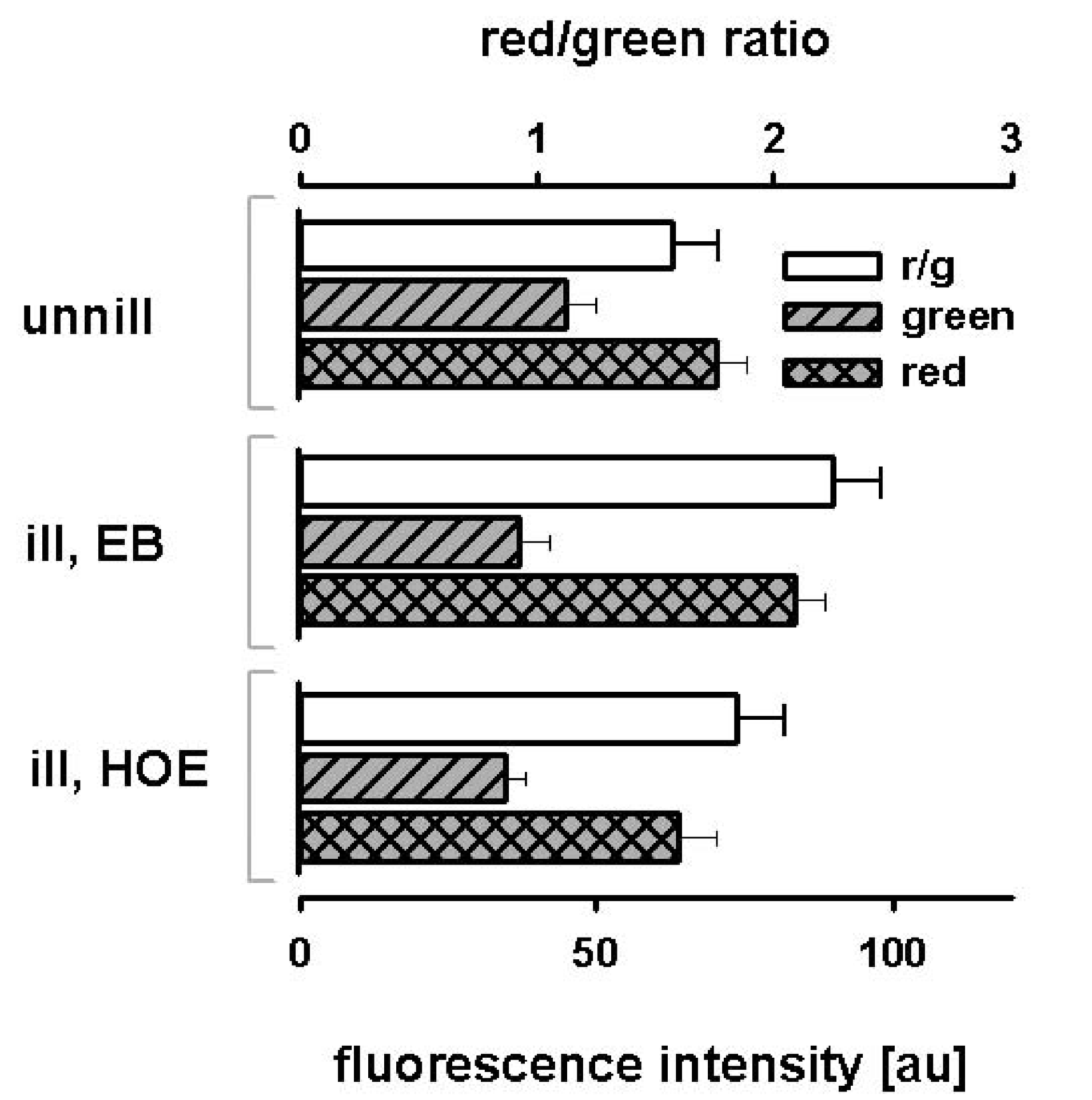
red/green ratio
0
1
2
3
unnill
ill, EB
ill, HOE
r/g
green
red
0
50
100
fluorescence intensity [au]